CHEMISTRY

Neat monolayer tiling of molecularly thin two-dimensional materials in 1 min

Kazuaki Matsuba,* Chengxiang Wang,* Kazuko Saruwatari, Yusuke Uesusuki, Kosho Akatsuka, Minoru Osada, Yasuo Ebina, Renzhi Ma, Takayoshi Sasaki†

Controlled arrangement of molecularly thin two-dimensional (2D) materials on a substrate, particularly into precisely organized mono- and multilayer structures, is a key to design a nanodevice using their unique and enhanced physical properties. Several techniques such as mechanical transfer process and Langmuir-Blodgett deposition have been applied for this purpose, but they have severe restrictions for large-scale practical applications, for example, limited processable area and long fabrication time, requiring skilled multistep operations. We report a facile one-pot spin-coating method to realize dense monolayer tiling of various 2D materials, such as graphene and metal oxide nanosheets, within 1 min over a wide area (for example, a 30-mmϕ substrate). Centrifugal force drives the nanosheets in a thin fluid layer to the substrate edge where they are packed edge to edge all the way to the central region, without forming overlaps. We investigated the relationship between precursor concentration, rotation speed, and ultraviolet-visible absorbance and developed an effective method to optimize the parameters for neat monolayer films. The multilayer buildup is feasible by repeating the spin-coating process combined with a heat treatment at moderate temperature. This versatile solution-based technique will provide both fundamental and practical advancements in the rapid large-scale production of artificial lattice-like films and nanodevices based on 2D materials.

INTRODUCTION

In recent years, intensive investigations have been conducted to develop a variety of molecularly thin two-dimensional (2D) materials, ranging from graphene, boron nitride, and metal dichalcogenides to oxides, hydroxides, and others (*1*, *2*), which exhibit unprecedented properties, such as high carrier mobility (*3*), enhanced catalytic activity (*4*), and size effect–free high permittivity (*5*). To fully use these functionalities, the primary issue of organizing the nanosheets into a highly controlled nanostructure should be resolved, and various techniques have been developed. Among them, the so-called mechanical transfer is the most used method that allows the manipulation of 2D objects, generally in micrometer-scale size, into a specific position on a substrate (*6*, *7*). This process, combined with modern nanofabrication techniques, such as photolithography, has been widely applied to design a "nanodevice" comprised of a single nanosheet or of a stack of a few sheets with intriguing electronic, optical, or quantum properties (*8*, *9*). This process is, without doubt, of extreme importance, but its sheet-by-sheet manipulation limits the applicable scope primarily to physical property measurements.

In general, practical applications require the ordered arrangement of nanosheets over a wide area. One of the most elementary systems is a monolayer of densely packed nanosheets without gaps or overlaps. Ideally, such a monolayer could be assembled repeatedly into multilayers or even into complex superlattice-like structures.

Conventional solution-based techniques, such as spin coating, inkjet printing, and spray drying, have many advantages as practical processes for wide-area coating. However, their ability to control film architecture and thickness does not come close to meeting the above prerequisites. In contrast, electrostatic self-assembly and Langmuir-Blodgett (LB) procedures enable layer-by-layer deposition of well-packed nanosheets into diverse nanoarchitectures (*10*–*14*), providing new insight into lattice engineering similar to modern vapor-phase beam epitaxy techniques (*15*–*17*). This approach has created considerable opportunities for designing advanced and sophisticated functionalities. For example, multilayer films of Ti- and Nb-based oxide nanosheets showed superior dielectric and insulating properties even at a nanoscale thickness of ~10 nm (*5*). Furthermore, synergetic intersheet coupling was demonstrated in superlattice films with a designed sequence of multiple nanosheets, realizing unique electronic, magnetic, and photochemical functionalities (*18*–*22*). However, despite these potential features, they still show limitations for industrial applications, such as long processing times and complicated deposition operations requirung expert skills. On the other hand, a spin-coating process of chemically derived graphene was recently reported, yielding uniform transparent and conducting thin films ranging from 1 to 2 up to 30 layers in thickness (*23*). In addition, Kim *et al.* (*24*) demonstrated the formation of mosaic-like monolayer films of graphene oxide (GO) via spin coating of its aqueous dispersion. Nevertheless, wide applicability to other 2D materials, and the precise multilayer buildup through a sequential monolayer-by-monolayer spin-coating process, have not been demonstrated.

Here, we found that a range of submicrometer– to tens-of-micrometer–sized 2D nanosheets, such as metal oxides ($Ti_{0.87}O_2^{0.52-}$ and $Ca_2Nb_3O_{10}^-$), GO, and its reduced form (rGO), could be neatly tiled into a substantially ideal monolayer on various substrates via a 1-min spin-coating process using a dimethyl sulfoxide (DMSO) suspension. The tiling process involves a new chemistry for 2D colloidal materials in a centrifugal force field. Furthermore, multilayer buildup is readily possible via repeated monolayer coating, which shows potential for a new convenient way to produce high-quality 2D nanosheet films.

RESULTS

Figure 1A depicts DMSO suspensions of the nanosheets used for spin coating. The original aqueous suspensions of metal oxide nanosheets ($Ti_{0.87}O_2^{0.52-}$ and $Ca_2Nb_3O_{10}^-$) (see fig. S1), GO, and rGO were prepared according to previously reported procedures (see the Supplementary Materials) (*25*–*28*). Next, the suspensions were converted into the DMSO ones through sedimentation of all the nanosheets

International Center for Materials Nanoarchitectonics, National Institute for Materials Science, 1-1 Namiki, Tsukuba, Ibaraki 305-0044, Japan.
*These authors contributed equally to this work.
†Corresponding author. Email: sasaki.takayoshi@nims.go.jp

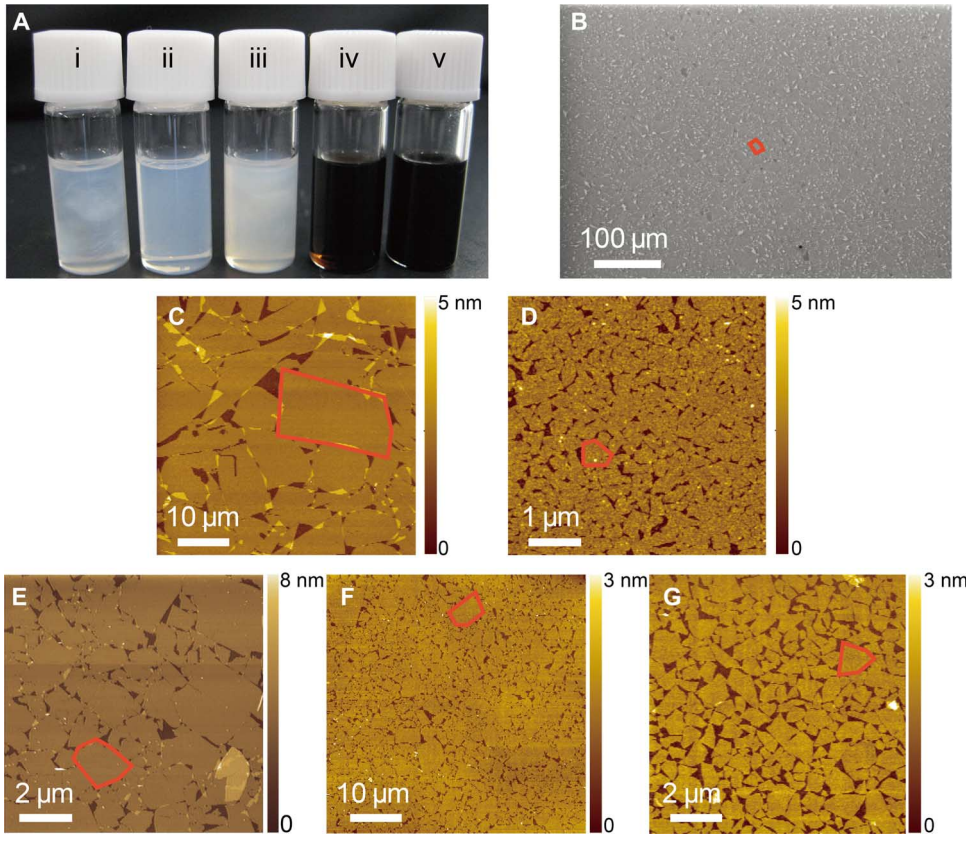

Fig. 1. Precursor suspensions for spin coating and the obtained monolayer films. (**A**) Typical precursor DMSO nanosheet suspensions for spin coating: Bottles i to v contain the suspensions of $Ti_{0.87}O_2^{0.52-}$ (large, 0.3 wt %), $Ti_{0.87}O_2^{0.52-}$ (small, 0.36 wt %), $Ca_2Nb_3O_{10}^-$ (1.38 wt %), GO (0.072 wt %), and rGO (0.045 wt %), respectively. (**B**) SEM image of the monolayer film obtained by spin coating the suspension of i. A single nanosheet is highlighted by a red polygon. (**C** to **G**) AFM images of the monolayer films via spin coating of the suspensions of i to v. The thickness of the nanosheets in (C) to (G) was ~1.4, 1.0, 2.3, 1.1, and 1.0 nm, respectively, which is consistent with the values reported for the unilamellar nanosheets. On the other hand, the average lateral size was ~10, 0.3, 2, 2, and 1 μm, respectively, which is compatible with the textural appearance of the suspensions.

via high-speed centrifugation followed by redispersion into DMSO. For the suspension of GO and rGO, we added an appropriate amount of tetrabutylammonium hydroxide (TBAOH) solution before redispersing in DMSO, which is a key to attain their neat tiling, as will be described below. DMSO is selected because of its appropriate viscosity as well as suspensibility of the nanosheets. The obtained suspensions of $Ti_{0.87}O_2^{0.52-}$ and $Ca_2Nb_3O_{10}^-$ nanosheets looked opalescent and translucent, whereas those of GO and rGO were black. The sample of large-size $Ti_{0.87}O_2^{0.52-}$ nanosheets (Fig. 1A, i) showed a clear schlieren texture from liquid crystallinity, reflecting their large lateral dimension, whereas the other samples of relatively small nanosheets showed a rather featureless appearance, evolving the texture only when agitated or turned around. The observable texture indicates that the nanosheets remained monodispersed in DMSO.

As seen from scanning electron microscopy (SEM) data (Fig. 1B and fig. S2), spin coating a DMSO suspension of large-size $Ti_{0.87}O_2^{0.52-}$ using optimized deposition parameters (40 μl, 3000 rpm) could cover the whole surface of a Si substrate with a nanosheet film. A nearly featureless image at a low magnification suggests uniform coverage. Surprisingly, atomic force microscopy (AFM) and high-magnification SEM data (Fig. 1C and fig. S2C) resolved individual nanosheets arranged edge to edge into a monolayer with negligible overlaps. The gaps were relatively noticeable but still limited, and a high coverage of >90% was attained. Comparably high-quality films could be fabricated with other nanosheets, small-size $Ti_{0.87}O_2^{0.52-}$, $Ca_2Nb_3O_{10}^-$, GO, and rGO, which differ in thickness, lateral size, and chemical characteristics (Fig. 1, D to G). Furthermore, the neatly tiled films could be obtained on various substrates, such as Si, Pt, and $SrTiO_3$ [Nb, 0.5 weight % (wt %)], in various size and shape (fig. S3). These results clearly indicate the wide applicability and versatility of this technique.

There are two important aspects to be noted: (i) TBA^+ ions are essential to attain the homogenous monolayer coating with neatly packed nanosheets. We could not achieve the neat tiling of $Ti_{0.87}O_2^{0.52-}$ nanosheets with a DMSO suspension derived from the sample exfoliated by a tetramethylammonium hydroxide solution (fig. S4). In addition, we failed to fabricate the monolayer films using the DMSO suspensions of GO and rGO without TBA^+ ions. Kim *et al.* (*24*) also pointed out the importance of TBA^+ ions for fabrication of the mosaic-like monolayer films of GO. (ii) DMSO is more suitable than aqueous suspensions as a coating medium. For example, the aqueous suspensions did not produce good films but resulted in patchy coating, contrasting to the films from the DMSO suspensions.

The film quality realizing the atomically flat surface topography with a roughness of 0.2 to 0.4 nm is comparable to that of the LB films (*13*, *14*). The obvious benefit is its inherently simple operation and short processing time. Typically, a monolayer coating can be completed in 1 min. In contrast, LB transfer usually takes more than 1 hour, except the LB scooping method recently developed by Archer and co-workers

(*29*, *30*) that enables much faster nanomaterial coating and does not require any mechanical barrier.

An AFM analysis was conducted on a series of locations in the film of large-size $Ti_{0.87}O_2^{0.52-}$, fabricated on a Si substrate (30 mmϕ) to obtain a closer view of their packing (Fig. 2). Obviously, the monolayer coverage dominated the major central area. Within a radius of 8 mm from the center, the film was clean and uniform. Note that this central area nearly corresponds to the uniform blue-colored area, which appeared in the final stage of the spin coating (Fig. 2, left). On the other hand, in the peripheral zone at 10 to 14 mm away from the center, an increasing number of overlaps are found, which provides an important hint for the film formation, as will be described.

Finding the proper deposition parameters to achieve monolayer coverage is critically important. Figure 3 illustrates the deposited amount of small- and large-size $Ti_{0.87}O_2^{0.52-}$ nanosheets as a function of two decisive factors, the nanosheet concentration (*C*), and the rotation speed (ω) when performing spin coating on a quartz glass substrate. The deposited amount can be conveniently monitored by the optical absorption at 265 nm from the nanosheet. A good linear relationship was obtained in plots of absorbance versus *C* and log(absorbance) versus log(ω) for the nanosheets. Therefore, the former correlation can be expressed as absorbance $\propto C$, and the latter can be expressed as log(absorbance) $\propto$ –log(ω) or absorbance $\propto \omega^{-\alpha}$. Consequently, absorbance $\propto C\,\omega^{-\alpha}$. This empirical correlation is compatible with the theoretical prediction as an approximation at low concentrations (see the Supplementary Materials). The blue zone in Fig. 3 indicates the absorbance (0.065 to 0.075) that was observed for the monolayer film of $Ti_{0.87}O_2^{0.52-}$ nanosheets constructed by the LB process (*14*). Thus, we can select sets of optimum parameters, *C* and ω, from the blue region to attain the monolayer coverage.

It is interesting to investigate how the nanosheets are arranged into the neatly tiled monolayer. Figure 4 shows a series of photographs in the typical spin-coating process of the small-size $Ti_{0.87}O_2^{0.52-}$ nanosheets. Upon initiation of rotation, a noticeable iridescent color with a regular ring pattern appeared, which should be due to optical interference from a thin layer of the nanosheet suspension on the substrate. The progressive change of the interference pattern with time can be ascribed to a gradual thinning of the fluid layer. Note that the wide central region showed a uniform pink color after 15 s, which then turned to orange and blue. This observation suggests that a homogenous area, known as the equal thickness region, developed at the center of the substrate. This uniform thin fluid layer continually becomes thinner. The observed colors disappeared after 45 s. In contrast, the edge region had rings in multiple colors, indicating the increasing fluid layer thickness toward the substrate end.

To obtain quantitative insight, we recorded the coating process under a monochromatic light of a Na lamp (λ = 589 nm). As shown in fig. S5, characteristic interference rings were clearly observed. We analyzed the number of the rings and their intervals, which changed with the progress of the spin coating, based on the standard equation for optical interference (fig. S6). The analysis revealed that the thickness of the fluid layer became thinner than 4 μm by 10 s after the start of the rotation. The thickness quickly decreased with time, becoming as low as ~120 nm.

Here, we discuss the formation of the nanosheet film on the basis of these observations. As schematically depicted in Fig. 4B, when the suspension is loaded on a substrate, it should spontaneously form a fluid layer in a concave upward shape in which nanosheets are monodispersed in a random orientation. Upon rotation, the fluid flows out from the substrate edge by the centrifugal force, and the fluid layer shape changes to downward concave. With the continuous loss of the fluid via spin coating and evaporation, the fluid layer becomes thinner and nearly flat except for the peripheral region. The nanosheets, which have a very high 2D aspect ratio, are forced to align in the radial flow direction and in parallel to the substrate in such a thin fluid layer under the centrifugal field. Another important factor to take into account is that the nanosheet surface is most likely covered with TBA ions, and the substrate surface used in these experiments is generally negatively charged. Thus, some of the nanosheets settle out onto the substrate due to electrostatic interactions; they then slide to the substrate edge because of the centrifugal force, where they are packed edge by edge due to a stopping effect of the fluid pool. Owing to the electrostatic repulsion between the

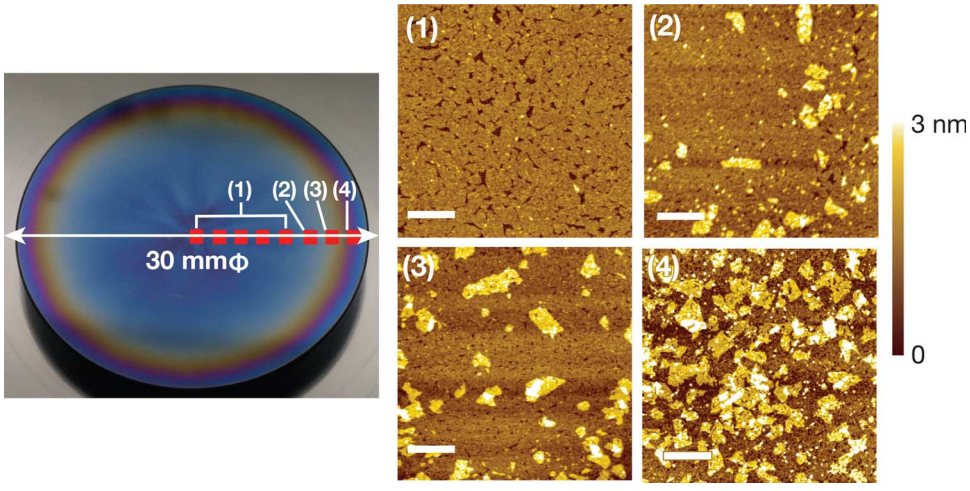

Fig. 2. AFM images of the monolayer film of small-size $Ti_{0.87}O_2^{0.52-}$ nanosheets along the radial direction. Images [(1) to (4)] on the left represent different positions (0 to 8, 10, 12, and 14 mm, respectively), away from the center of the substrate, and the corresponding AFM images are shown on the right. Scale bars, 1 μm. Within a radius of 8 mm from the center, the film was clean and uniform. Note that this central area nearly corresponds to the uniform blue area or the equal thickness region, which appeared in the final stage of the spin coating (left photograph). On the other hand, in the peripheral zone from 10 to 14 mm away from the center, an increasing number of overlaps was found.

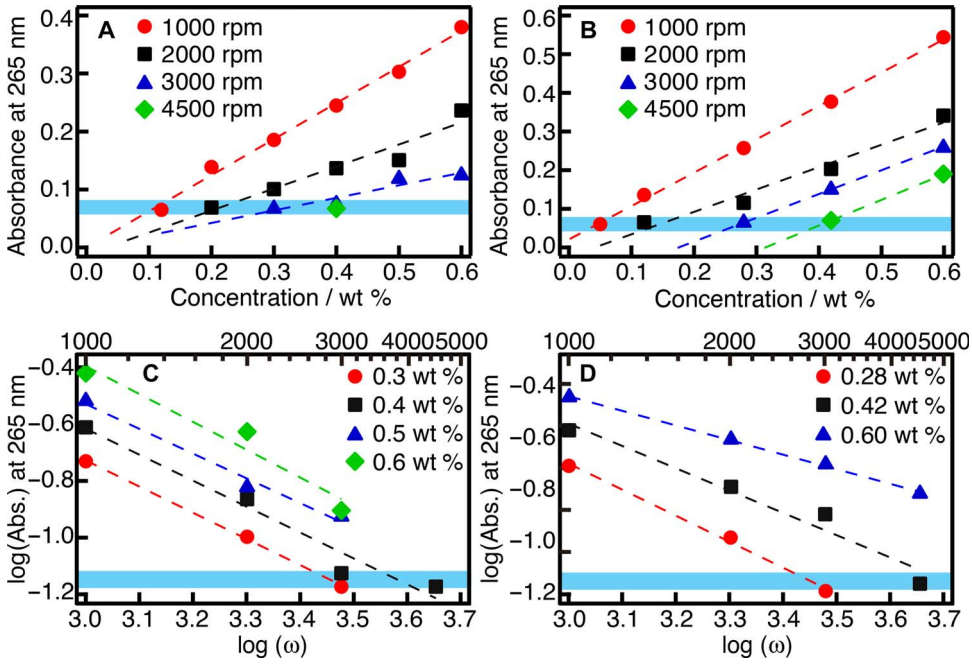

Fig. 3. Relationships between the absorbance at 265 nm of spin-coated films of $Ti_{0.87}O_2^{0.52-}$ nanosheets and the nanosheet concentration and rotation speed. (**A** and **C**) Small- size $Ti_{0.87}O_2^{0.52-}$ nanosheets. (**B** and **D**) Large-size $Ti_{0.87}O_2^{0.52-}$ nanosheets. The absorbance at 265 nm corresponds to the peak value of the absorption band of the nanosheets. The blue belts mark the absorbance range for monolayer films of $Ti_{0.87}O_2^{0.52-}$ nanosheets (0.065 to 0.075). Determining the intersections between the fitted lines and the blue belts provides the proper parameters.

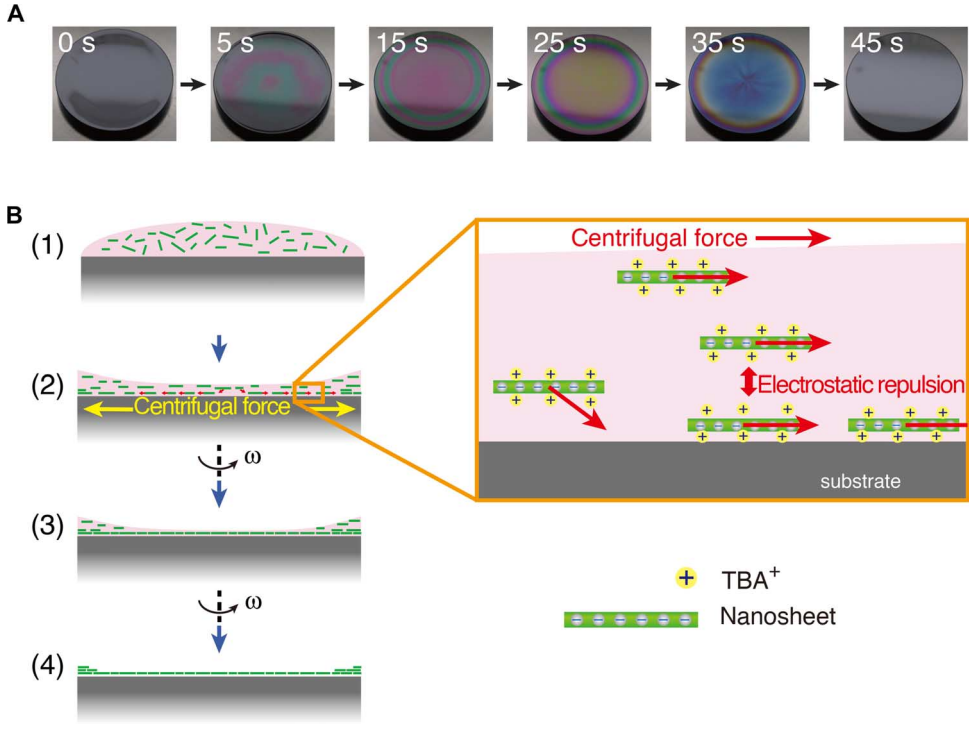

Fig. 4. Evolution of the spin-coating process and schematics of the edge-by-edge assembly of nanosheets. (**A**) Photographs of the spin-coating process with the suspension (40 μl, 0.40 wt %) of small-size $Ti_{0.87}O_2^{0.52-}$ nanosheets at a rotation speed of 4500 rpm. The transition of the interference patterns indicates the gradual thinning of the suspension layer. (**B**) A plausible model for the formation of the monolayer film of neatly tiled nanosheets.

nanosheets at the surface and in the fluid as well as their low population (approximately one sheet in the aforementioned 120-nm-thick DMSO layer), overlapped deposition is suppressed in the thin fluid layer. Accordingly, the nanosheets are packed sequentially into a monolayer from the edge to the central region, realizing the neatly tiled arrangement upon total loss of the solvent. This mechanism is supported by

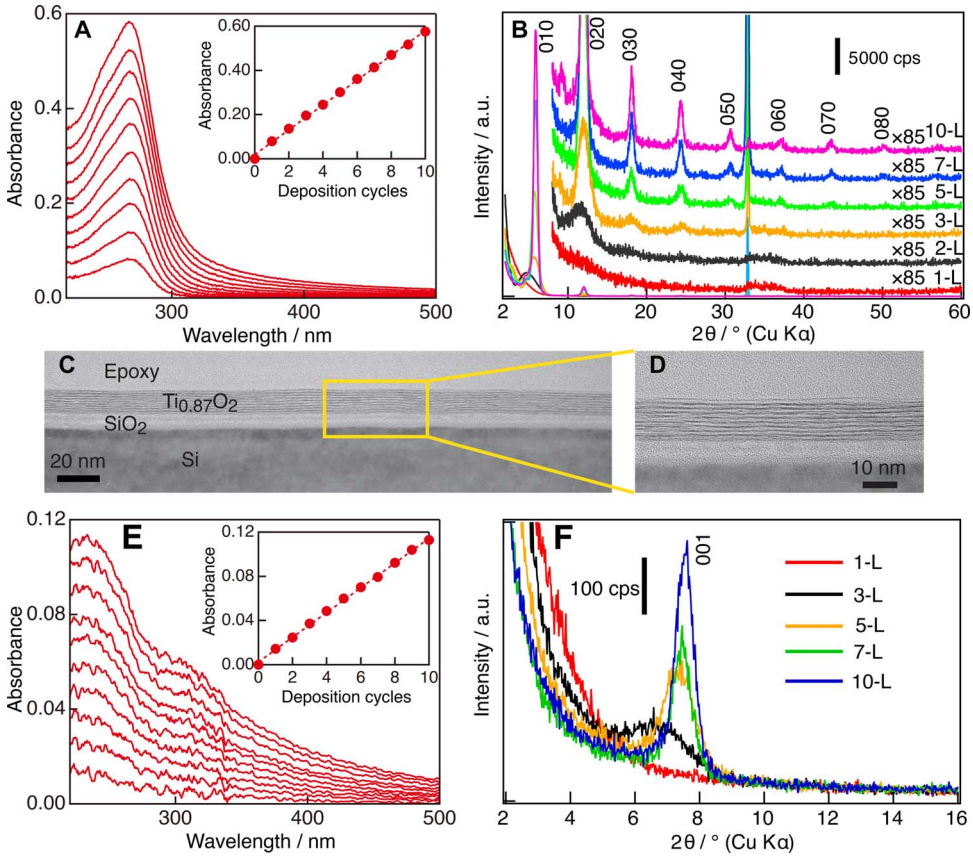

Fig. 5. Multilayer buildup process. (**A**) UV-visible absorption spectra of $Ti_{0.87}O_2^{0.52-}$ nanosheet films fabricated by repeating the monolayer coverage on a quartz glass substrate. (**B**) XRD patterns of $Ti_{0.87}O_2^{0.52-}$ nanosheet films with 1, 2, 3, 5, 7, and 10 layers (L) on a Si substrate. The profiles between 2° and 60° were magnified 85 times for clear observation. a.u., arbitrary units; cps, counts per second. (**C** and **D**) Cross-sectional HRTEM images of the 10-layer film of $Ti_{0.87}O_2^{0.52-}$ nanosheet on a Si substrate. (**E**) UV-visible absorption spectra from GO nanosheet films fabricated by repeating the monolayer coverage. (**F**) XRD patterns of GO nanosheet films with 1, 3, 5, 7, and 10 layers on a Si substrate.

the observations that the packing density of the nanosheets is higher at the edge than at the center, and that an uncovered area was formed in the central region when spin-coated with an insufficient amount of nanosheets.

The films thus fabricated show potential for various applications. For example, the film of $Ti_{0.87}O_2^{0.52-}$ exhibited high photoinduced superhydrophilicity upon exposure to ultraviolet (UV) light (fig. S7). Although the film is 1 nm thick, its activity was comparable to that of much thicker films of bulk anatase, which are widely used as the photocatalytic coating material (*31*). Furthermore, the glass substrate covered with the nanosheets promoted the oriented growth of a $SrTiO_3$ film along the [110] axis via pulsed laser deposition (fig. S8), indicating the seed layer effect. A great benefit for such a deposition is that substrates of amorphous materials, such as glass and plastics, can be used like a single-crystal substrate for epitaxial film growth, once coated with appropriate nanosheets (*32*).

Construction of multilayer nanosheet films is also of significant importance with respect to their practical applications, including high-*k* dielectric nanofilms (*5*). We successfully demonstrated multilayer buildup by basically repeating the spin coating. One major caution to be taken was fixing the nanosheets tightly enough to the substrate for them not to be peeled off in the following coating steps. Using a slow rotation speed and an appropriate nanosheet concentration was essential. In addition, heating the film to 100° to 200°C was effective in improving its binding to substrates.

Figure 5 (A and B) shows x-ray diffraction (XRD) data and UV-visible absorption spectra when we repeated spin coating for large-size $Ti_{0.87}O_2^{0.52-}$ nanosheets as a typical example. The rather slow rotation speed of 1600 rpm was used, and the sample was washed with water after each deposition, followed by heating at 200°C for 20 min. The absorption peak at 265 nm attributable to the nanosheet was linearly enhanced as a function of coating cycles, clearly indicating the regular film growth. XRD data showed the evolution of basal diffraction peaks having a *d* value of ~1.4 nm, which can be ascribed to the lamellar structure of $Ti_{0.87}O_2^{0.52-}$ nanosheets accommodating TBA ions as well as DMSO in the galleries. Through repeating the coating cycles, the peaks became more intense and sharper, strongly supporting the layer-by-layer growth of the film. The 10-layer film showed very sharp basal peaks up to the eighth order. The coherent length was estimated as ~15 nm by Scherrer's equation, being comparable to the film thickness. The coherency over the whole film was taken as a proof of high structural order, as previously reported for the LB film (*14*). High-resolution transmission electron microscopy (HRTEM) resolved the lamellar fringes from the nanosheets coated layer by layer (Fig. 5, C and D), also revealing the uniform and highly ordered architecture of the film.

We also constructed 10-layer films of GO nanosheets $[(GO)_{10}]$ on Si wafers. The evolution of the XRD peak and UV-visible absorption profile (Fig. 5, E and F) again provides a compelling evidence for the successful multilayer buildup. These data indicate the formation of well-developed homogeneous multilayer films, which is essentially

important to develop nanodevices fully using unique aspects of 2D nanosheets.

DISCUSSION

We have demonstrated the rapid fabrication of highly organized mono-/multilayer films from various 2D materials by a handy spin-coating method. There are two prerequisites to be noted for the successful implementation of this process. First, DMSO is a more robust medium to support spin coating of variable nanosheets, whereas the common aqueous medium cannot. Until now, only GO monolayer film was realized by spin coating in aqueous medium as reported by Kim *et al.* (*24*). We showed that aqueous suspensions of TBAOH-exfoliated $Ti_{0.87}O_2^{0.52-}$ or $Ca_2Nb_3O_{10}^-$ nanosheets were not suitable for the spin coating to obtain their neat monolayer films, instead there are a large amount of overlaps, or the nanosheets stack together rather than form a uniform monolayer. The success of DMSO might be due to its proper viscosity that prohibits nanosheets from spreading out too quickly in the spin-coating process and its suitably slow evaporation rate that timely settles nanosheets on substrates after spreading uniformly. In addition, the excellent dispersibility makes DMSO applicable for suspending nanosheets in a different solvent other than water. Second, TBA^+ seems at least necessary for the present three kinds of nanosheets. The role of TBA^+ should not simply prevent the nanosheets from aggregating together. When using TMA^+ in place of TBA^+, all the nanosheets examined underwent severe overlaps. In the case of TBA-coated GO, Kim *et al.* (*24*) argued that TBA^+ modification weakens the edge-to-edge repulsion of nanosheets and promotes the disruption of hydrogen bond connecting basal planes of parallel nanosheets, which favors the formation of monolayer film rather than multilayer film. Further considerations may be needed to understand the role of TBA^+ because TMA^+ also has the similar effects like TBA^+. A plausible explanation is based on different dimensions and resultant electrostatic interactions (that is, different charge-to-size ratio) of these cations. To achieve a neat tiling, the nanosheets must be able to slide on the substrate to the edge under a centrifugal force, which requires a relatively weak electrostatic interaction between the nanosheets and the substrate surface moderated by the cations. TBA^+ seems to meet the requirements due to its suitable charge-to-size ratio. TMA^+ has a smaller dimension than TBA^+, yielding a relatively strong binding force, which might prevent the nanosheets from rapidly migrating over the substrate surface. As a result, serious overlapped regions were observed. On the other hand, cations larger than TBA^+ may also fail because the binding force might be too weak to effectively settle nanosheets on the substrate.

The monolayer formation of TBA^+-coated nanosheets on the substrate should be logically considered as a progressive assembly process from the edge to the center, which is in accordance with the AFM observations. It means that the formation of monolayer film finished at the center, where a loosely packed nanosheet film was probably formed. In this regard, to finally prepare a closely packed monolayer film, it is required that the nanosheet suspension should not spread out too quickly by centrifugal force before forming a closely packed film at the center, which implies the importance of the viscosity of solvent and the concentration of nanosheet suspension. In addition, maintaining nanosheets is also dependent on the evaporation rate of solvent, rotation speed, etc. The high rotation speed is conducive to make a more densely packed film but leads to a larger evaporation rate and quicker removing rate by centrifugal force. For the above reasons, we need to adjust the rotation speed and nanosheet concentration to obtain an ideal monolayer film if the DMSO medium is used.

Spin coating has been widely used in the semiconductor industry due to its simplicity and feasibility. The highly efficient preparation of nanosheet films via spin coating, achieving monolayer tiling of nanosheets comparable to LB, certainly shows potential as a great application prospect, although there are still technological hurdles (for example, scaling up to larger substrate sizes) needed to be addressed before any practical use.

MATERIALS AND METHODS

Preparation of DMSO nanosheet dispersions for spin coating $Ti_{0.87}O_2^{0.52-}$ and $Ca_2Nb_3O_{10}^-$

The aqueous suspension of exfoliated $Ti_{0.87}O_2^{0.52-}$ nanosheets was first centrifuged at a low speed of 1500 rpm for 15 min. After removing a small amount of the sedimented unexfoliated material, the remaining suspension was subjected to high-speed centrifugation (30,000 rpm for 30 min) to recover all the nanosheets. The top supernatant aqueous solution was discarded, and the sediment at the bottom was resuspended into different volumes of DMSO to prepare precursor suspensions with varied contents (0.14, 0.2, 0.3, 0.4, 0.5, and 0.6 wt % for small-size nanosheets and 0.05, 0.12, 0.28, 0.42, and 0.60 wt % for large-size nanosheets).

A similar procedure was applied to $Ca_2Nb_3O_{10}^-$. The unexfoliated material was removed from the colloidal suspension (30 cm^3) of $Ca_2Nb_3O_{10}^-$ nanosheets by applying low-speed centrifugation at 3000 rpm for 10 min. Then, the upper suspension was transferred to a new tube and centrifuged again at 15,000 rpm for 30 min. The nanosheets sedimented at the bottom were resuspended into DMSO (20 cm^3). This process was repeated several times to eliminate water from the suspension. Finally, the purified $Ca_2Nb_3O_{10}^-$ nanosheets were dispersed into DMSO (5 cm^3) to achieve a nanosheet content of 1.38 wt %. The obtained suspension was used directly or after appropriately diluting with DMSO for spin coating.

Graphene oxide

An aliquot (5 cm^3) of a diluted TBAOH solution (0.5 wt %) was slowly dropped into 20 cm^3 of the pristine GO suspension to obtain a pH value of ~10.2. The mixture was sonicated for 5 min and then centrifuged at 3000 rpm for 10 min to remove any unexfoliated graphite and other possible impurities. Then, the upper suspension was centrifuged again at 15,000 rpm for 30 min, and the sediment at the bottom was redispersed in DMSO to the total volume of 20 cm^3. The resulting suspension with a GO content of ~0.072 wt % was used in the spin-coating experiments. Usually, the ultrasonic treatment was applied to the sample for 10 min before spin coating to attain a good dispersion.

Reduced graphene oxide

The rGO nanosheets obtained as a suspension in formamide through the chemical reduction process were separated by centrifugation at 25,000 rpm for 30 min and resuspended into DMSO to produce a new suspension of 0.045 wt %. Then, 1.5 cm^3 of TBAOH solution (1.0 wt %) was slowly added, and this mixture was centrifuged again at 25,000 rpm for 30 min. The obtained sediment was resuspended into DMSO to produce the final precursor for spin coating with a concentration of 0.045 wt %.

Deposition of monolayer films

Typically, circular plates (30 mmϕ of Si and quartz glass) were used as substrates for spin coating. The substrates were cleaned by immersing them in a mixed solution of CH_3OH/HCl [1:1 (v/v)] and concentrated

H_2SO_4 for 30 min each. Then, the DMSO nanosheet dispersion, either $Ti_{0.87}O_2^{0.52-}$ (40 μl), GO (40 μl), or $Ca_2Nb_3O_{10}^-$ (20 μl), was loaded onto the cleaned substrate and spin-coated at a certain rotation speed in a clean room booth (Class 1000) regulated at 26°C. After drying, the films fabricated on the Si substrate were characterized with AFM or SEM, and those on the quartz glass slide were examined by UV-visible absorption spectroscopy.

Fabrication of multilayer films

Multilayer films of GO and large-size $Ti_{0.87}O_2^{0.52-}$ nanosheets were fabricated. Their monolayer films were deposited according to the procedures described above. Before depositing the next layer, the as-fabricated $Ti_{0.87}O_2^{0.52-}$ and GO nanosheet films were heated in air at 200°C for 20 min and 110°C for 5 min, respectively. For $Ti_{0.87}O_2^{0.52-}$ nanosheets, the heated film was washed with Milli-Q water to turn the surface hydrophilic. Multilayer films of $(Ti_{0.87}O_2^{0.52-})_n$ and $(GO)_n$ were constructed by repeating the above process for n times.

SUPPLEMENTARY MATERIALS

Supplementary material for this article is available at http://advances.sciencemag.org/cgi/content/full/3/6/e1700414/DC1

section S1. Synthesis of $Ti_{0.87}O_2^{0.52-}$, $Ca_2Nb_3O_{10}^-$, GO, and rGO nanosheets

section S2. Characterizations of nanosheet films

section S3. Derivation of the dependence of the absorbance on the concentration and rotation speed

fig. S1. Schematic representation for 2D materials used in this study.

fig. S2. Photograph and SEM images of the Si substrate (30 mmϕ) after spin coating the DMSO suspension of large-size $Ti_{0.87}O_2^{0.52-}$.

fig. S3. SEM images of monolayer films of large-size $Ti_{0.87}O_2^{0.52-}$ nanosheets on various substrates.

fig. S4. AFM images of monolayer films.

fig. S5. Photographs of the spin-coating process.

fig. S6. The schematic of the optical path to calculate the nanosheet suspension thickness.

fig. S7. Contact angle of a water droplet on the monolayer film of large-size $Ti_{0.87}O_2^{0.52-}$ nanosheets upon exposure to UV light.

fig. S8. XRD data of $SrTiO_3$ film grown on the monolayer film of large-size $Ti_{0.87}O_2^{0.52-}$ nanosheets.

fig. S9. XRD patterns of dried samples of GO and rGO.

References (*33*, *34*)

REFERENCES AND NOTES

1. S. Z. Bulter, S. M. Hollen, L. Cao, Y. Cui, J. A. Gupta, H. R. Gutiérrez, T. F. Heinz, S. S. Hong, J. Huang, A. F. Ismach, E. Johnston-Halperin, M. Kuno, V. V. Plashnitsa, R. D. Robinson, R. S. Ruoff, S. Salahuddin, J. Shan, L. Shi, M. G. Spencer, M. Terrones, W. Windl, J. E. Goldberger, Progress, challenges, and opportunities in two-dimensional materials beyond graphene. *ACS Nano* **7**, 2898–2926 (2013).
2. R. Ma, T. Sasaki, Nanosheets of oxides and hydroxides: Ultimate 2D charge-bearing functional crystallites. *Adv. Mater.* **22**, 5082–5104 (2010).
3. K. Kim, J.-Y. Choi, T. Kim, S.-H. Cho, H.-J. Chung, A role for graphene in silicon-based semiconductor devices. *Nature* **479**, 338–344 (2011).
4. D. Voiry, H. Yamaguchi, J. Li, R. Silva, D. C. B. Alves, T. Fujita, M. Chen, T. Asefa, V. B. Shenoy, G. Eda, M. Chhowalla, Enhanced catalytic activity in strained chemically exfoliated WS_2 nanosheets for hydrogen evolution. *Nat. Mater.* **12**, 850–855 (2013).
5. M. Osada, T. Sasaki, Two-dimensional dielectric nanosheets: Novel nanoelectronics from nanocrystal building blocks. *Adv. Mater.* **24**, 210–228 (2012).
6. C. R. Dean, A. F. Young, I. Meric, C. Lee, L. Wang, S. Sorgenfrei, K. Watanabe, T. Taniguchi, P. Kim, K. L. Shepard, J. Hone, Boron nitride substrates for high-quality graphene electronics. *Nat. Nanotechnol.* **5**, 722–726 (2010).
7. J. Song, F.-Y. Kam, R.-Q. Png, W.-L. Seah, J.-M. Zhuo, G.-K. Lim, P. K. H. Ho, L.-L. Chua, A general method for transferring graphene onto soft surfaces. *Nat. Nanotechnol.* **8**, 356–362 (2013).
8. G. Fiori, F. Bonaccorso, G. Iannaccone, T. Palacios, D. Neumaier, A. Seabaugh, S. K. Banerjee, L. Colombo, Electronics based on two-dimensional materials. *Nat. Nanotechnol.* **9**, 768–779 (2014).
9. L. Gao, G.-X. Ni, Y. Liu, B. Liu, A. H. Castro Neto, K. P. Loh, Face-to-face transfer of wafer-scale graphene films. *Nature* **505**, 190–194 (2014).
10. S. W. Keller, H.-N. Kim, T. E. Mallouk, Layer-by-layer assembly of intercalation compounds and heterostructures on surfaces: Toward molecular "beaker" epitaxy. *J. Am. Chem. Soc.* **116**, 8817–8818 (1994).
11. T. Tanaka, K. Fukuda, Y. Ebina, K. Takada, T. Sasaki, Highly organized self-assembled monolayer and multilayer films of titania nanosheets. *Adv. Mater.* **16**, 872–875 (2004).
12. N. A. Kotov, F. C. Meldrum, J. H. Fendler, E. Tombácz, I. Dékány, Spreading of clay organocomplexes on aqueous solutions: Construction of Langmuir-Blodgett clay organocomplex multilayer films. *Langmuir* **10**, 3797–3804 (1994).
13. L. J. Cote, F. Kim, J. Huang, Langmuir–Blodgett assembly of graphite oxide single layers. *J. Am. Chem. Soc.* **131**, 1043–1049 (2009).
14. K. Akatsuka, M. Haga, Y. Ebina, M. Osada, K. Fukuda, T. Sasaki, Construction of highly ordered lamellar nanostructures through Langmuir–Blodgett deposition of molecularly thin titania nanosheets tens of micrometers wide and their excellent dielectric properties. *ACS Nano* **3**, 1097–1106 (2009).
15. G. Rijnders, D. H. A. Blank, Build your own superlattice. *Nature* **433**, 369–370 (2005).
16. B. V. Lotsch, Vertical 2D heterostructures. *Annu. Rev. Mater. Res.* **45**, 85–109 (2015).
17. R. Ma, T. Sasaki, Two-dimensional oxide and hydroxide nanosheets: Controllable high quality exfoliation, molecular assembly, and exploration of functionality. *Acc. Chem. Res.* **48**, 136–143 (2015).
18. D. M. Kaschak, J. T. Lean, C. C. Waraksa, G. B. Saupe, H. Usami, T. E. Mallouk, Photoinduced energy and electron transfer reactions in lamellar polyanion/polycation thin films: Toward an inorganic "leaf". *J. Am. Chem. Soc.* **121**, 3435–3445 (1999).
19. N. Sakai, K. Fukuda, Y. Omomo, Y. Ebina, K. Takada, T. Sasaki, Hetero-nanostructured films of titanium and manganese oxide nanosheets: Photoinduced charge transfer and electrochemical properties. *J. Phys. Chem. C* **112**, 5197–5202 (2008).
20. B.-W. Li, M. Osada, T. C. Ozawa, Y. Ebina, K. Akatsuka, R. Ma, H. Funakubo, T. Sasaki, Engineered interfaces of artificial perovskite oxide superlattices via nanosheet deposition process. *ACS Nano* **4**, 6673–6680 (2010).
21. C. Ziegler, S. Werner, M. Bugnet, M. Wörsching, V. Duppel, G. A. Botton, C. Scheu, B. V. Lotsch, Artificial solids by design: Assembly and electron microscopy study of nanosheet-derived heterostructures. *Chem. Mater.* **25**, 4892–4900 (2013).
22. B.-W. Li, M. Osada, Y. Ebina, S. Ueda, T. Sasaki, Coexistence of magnetic order and ferroelectricity at 2D nanosheet interfaces. *J. Am. Chem. Soc.* **138**, 7621–7625 (2016).
23. H. Yamaguchi, G. Eda, C. Mattevi, H. K. Kim, M. Chhowalla, Highly uniform 300 mm wafer-scale deposition of single and multilayered chemically derived graphene thin films. *ACS Nano* **4**, 524–528 (2010).
24. J. W. Kim, D. Kang, T. H. Kim, S. G. Lee, N. Byun, D. W. Lee, B. H. Seo, R. S. Ruoff, H. S. Shin, Mosaic-like monolayer of graphene oxide sheets decorated with tetrabutylammonium ions. *ACS Nano* **7**, 8082–8088 (2013).
25. T. Sasaki, M. Watanabe, H. Hashizume, H. Yamada, H. Nakazawa, Macromolecule-like aspects for a colloidal suspension of an exfoliated titanate. Pairwise association of nanosheets and dynamic reassembling process initiated from it. *J. Am. Chem. Soc.* **118**, 8329–8335 (1996).
26. R. E. Schaak, T. E. Mallouk, Perovskites by design: A toolbox of solid-state reactions. *Chem. Mater.* **14**, 1455–1471 (2002).
27. W. S. Hummers Jr., R. E. Offeman, Preparation of graphitic oxide. *J. Am. Chem. Soc.* **80**, 1339–1339 (1958).
28. V. C. Tung, M. J. Allen, Y. Yang, R. B. Kaner, High-throughput solution processing of large-scale graphene. *Nat. Nanotechnol.* **4**, 25–29 (2009).
29. M. S. Kim, L. Ma, S. Choudhury, S. S. Moganty, S. Wei, L. A. Archer, Fabricating multifunctional nanoparticle membranes by a fast layer-by-layer Langmuir–Blodgett process: Application in lithium–sulfur batteries. *J. Mater. Chem. A* **4**, 14709–14719 (2016).
30. M. S. Kim, L. Ma, S. Choudhury, L. A. Archer, Multifunctional separator coatings for high-performance lithium–sulfur batteries. *Adv. Mater. Interfaces* **3**, 1600450 (2016).
31. N. Sakai, K. Fukuda, T. Shibata, Y. Ebina, K. Takada, T. Sasaki, Photoinduced hydrophilic conversion properties of titania nanosheets. *J. Phys. Chem. B* **110**, 6198–6203 (2006).
32. T. Shibata, H. Takano, Y. Ebina, D. S. Kim, T. C. Ozawa, K. Akatsuka, T. Ohnishi, K. Takada, T. Kogure, T. Sasaki, Versatile van der Waals epitaxy-like growth of crystal films using two-dimensional nanosheets as a seed layer: Orientation tuning of $SrTiO_3$ films along three important axes on glass substrates. *J. Mater. Chem. C* **2**, 441–449 (2014).
33. N. Sahu, B. Parija, S. Panigrahi, Fundamental understanding and modeling of spin coating process: A review. *Indian J. Phys.* **83**, 493–502 (2009).
34. D. Meyerhofer, Characteristics of resist films produced by spinning. *J. Appl. Phys.* **49**, 3993–3997 (1978).

Acknowledgments

Funding: T.S. acknowledges the support from the World Premier International Research Center Initiative on Materials Nanoarchitectonics, the Ministry of Education, Culture, Sports, Science and Technology (Japan), and the Core Research for Evolutional Science and Technology, Japan Science and Technology Agency. **Author contributions:** K.M., Y.U., C.W., and K.S. performed the spin coating and collected the data of $Ti_{0.87}O_2^{0.52-}$, GO, rGO, and $Ca_2Nb_3O_{10}^-$ nanosheets, and T.S. supervised the research. K.A. helped guide the synthesis of $Ti_{0.87}O_2^{0.52-}$ nanosheet. M.O. assisted in the HRTEM studies. Y.E. helped guide the synthesis of $Ca_2Nb_3O_{10}^-$ nanosheet and assisted the AFM measurements. R.M. helped guide the

synthesis of GO and rGO nanosheets. C.W. interpreted the data with help from R.M. and T.S. C.W. and T.S. organized the paper. All authors contributed to this work. **Competing interests:** T.S., K.S., K.M., K.A., Y.E., and M.O. are authors on a patent related to this work issued by the Japan Patent Office (patent no. 5984089; U.S. patent no. US8,828,488 B2, 9 September 2014). The other authors declare that they have no competing interests. **Data and materials availability:** All data needed to evaluate the conclusions in the paper are present in the paper and/or the Supplementary Materials. Additional data related to this paper may be requested from the authors.

Submitted 7 February 2017
Accepted 9 May 2017
Published 30 June 2017
10.1126/sciadv.1700414

Citation: K. Matsuba, C. Wang, K. Saruwatari, Y. Uesusuki, K. Akatsuka, M. Osada, Y. Ebina, R. Ma, T. Sasaki, Neat monolayer tiling of molecularly thin two-dimensional materials in 1 min. *Sci. Adv.* **3**, e1700414 (2017).

Science Advances

Neat monolayer tiling of molecularly thin two-dimensional materials in 1 min

Kazuaki Matsuba, Chengxiang Wang, Kazuko Saruwatari, Yusuke Uesusuki, Kosho Akatsuka, Minoru Osada, Yasuo Ebina, Renzhi Ma and Takayoshi Sasaki

Sci Adv **3** (6), e1700414.
DOI: 10.1126/sciadv.1700414

Science Advances (ISSN 2375-2548) is published by the American Association for the Advancement of Science, 1200 New York Avenue NW, Washington, DC 20005. The title *Science Advances* is a registered trademark of AAAS.